Applied Catalysis B: Environmental 204 (2017) 561–565

Contents lists available at ScienceDirect

Applied Catalysis B: Environmental

journal homepage: www.elsevier.com/locate/apcatb

Clinical wastewater treatment: Photochemical removal of an anionic antibiotic (ciprofloxacin) by mesostructured high aspect ratio ZnO nanotubes

Carina Bojer[a], Judith Schöbel[b], Thomas Martin[a], Michael Ertl[a], Holger Schmalz[b], Josef Breu[a,*]

[a] Lehrstuhl für Anorganische Chemie I, Universität Bayreuth, 95440 Bayreuth, Germany
[b] Lehrstuhl für Makromolekulare Chemie II, Universität Bayreuth, 95440 Bayreuth, Germany

ARTICLE INFO

Article history:
Received 23 September 2016
Received in revised form
23 November 2016
Accepted 1 December 2016
Available online 5 December 2016

Keywords:
Wastewater treatment
Photocatalyst
Ciprofloxacin
ZnO nanotubes
Mesostructured

ABSTRACT

Zinc oxide (ZnO) nanoparticles were mesostructured by polybutadiene-*block*-poly(2-vinylpyridine) cylindrical polymer brushes as a template. Loading the positively charged vinylpyridine block with ZnO nanoparticles produced hybrid rods with high aspect ratio. Mesostructured ZnO nanotubes obtained by pyrolytic template removal show high activity in the photocatalytic degradation of ciprofloxacin using a continuous flow reactor and irradiation with terrestrial solar spectrum. In comparison with Degussa P25, a titanium dioxide photocatalyst, the degradation is 2.9 times faster. Due to its non-woven microstructure, the photocatalyst, moreover, can be easily separated from fluid reaction media by filtration.

1. Introduction

Active pharmaceutical ingredients like beta blockers, antiphlogistics or antibiotics have been detected in considerable quantities in wastewater and even in drinking water [1]. In Europe, the most commonly prescribed quinolone antibiotic is ciprofloxacin. It is applied to skin infections and sexually transmitted diseases [2]. Ciprofloxacin belongs to the family of fluoroquinolones and is a broad-spectrum antibacterial compound used in private households, veterinary medicine and hospitals. Focusing on hospitals a daily water consumption of 260–940 L per bed is usual. This wastewater has an antibiotics pollution e.g. with ciprofloxacin up to 101 $\mu g\,L^{-1}$ [3,4].

Clinical wastewater consequently needs pretreatment before it can be handled by community wastewater facilities triggering intensive research into methods and active catalysts for the degradation of these medical pollutants [5]. One promising approach is advanced oxidation processes (AOPs). In AOPs a reactive radical species is in situ generated by energy like solar energy, which is one of the most abundant clean energy sources available [6–8]. Promising photocatalysts in environmental waste management systems are amongst others titanium dioxide (TiO_2), zinc oxide (ZnO), iron(III) oxide (Fe_2O_3) or vanadium(V) oxide (V_2O_5) [9–11].

ZnO is an important direct wide bandgap II–VI semiconductor with a bandgap of 3.37 eV [12]. Its large exciton binding energy of 60 meV the good biocompatibility, low costs, strong oxidation ability and mechanical strength are reasons for the potential applications in photocatalysis [13–17].

2. Photocatalysis of ciprofloxacin in clinical wastewater treatment

Most active pharmaceutical ingredients are formulated as ions to assure solubility in body fluids. Therefore, very commonly carboxylate groups are introduced into the molecular structure and at pH values above ≈6 such molecules carry a negative charge [18]. Ciprofloxacin has its isoelectric point (zwitterion) at pH 7.4 resulting from the pK_a values of 6.09 for the carboxylic group and 8.74 for the nitrogen of the piperazinyl ring [19]. At the same time the surface of oxidic semiconductors also carries a negative charge above an pH value higher than the point of zero charge (PZC). For hospital wastewater typically an average pH of around 8 was determined

* Corresponding author.
E-mail address: josef.breu@uni-bayreuth.de (J. Breu).

http://dx.doi.org/10.1016/j.apcatb.2016.12.003
0926-3373/

[3,20]. It happens that this pH is between the PZC of rather acidic TiO_2 and more basic ZnO. Consequently, the surface of Degussa P25 (P25) with a PZC of 6.9 is negatively charged [21] while the ZnO surface with a PZC of 9.3 will be positively charged at the pH of typical hospital sewage [22]. Since, as mentioned above, ciprofloxacin is anionic in alkaline conditions, it is expected that adsorption of ciprofloxacin on the ZnO surface should be electrostatically favored contrary to the disfavored adsorption at the like-charged P25 surface. In this line, it has been reported that the photodegradation of the anionic pollutant RED-3BA on TiO_2 was more efficient at pH 4 compared with tests at pH 7 and pH 11, values above the PZC of TiO_2 where the surface of the photocatalyst become negatively charged [23].

While in a first approximation, efficiency increases with the surface area of the catalyst, photodegradation in a fluid medium like clinical wastewater treatment requires the separation from the wastewater e.g. by filtration or in continuous flow reactors. Consequently, mesostructuring of nanoparticles as applied in this work represents a good compromise between maximizing the catalyst surface and the possibility to separate or recycle the catalyst. Hence, it is necessary to build macroscopic structures of nanoparticles like nanotubular aggregates.

In this work, ZnO nanotubes were prepared by self-assembly of ZnO nanoparticles using electrostatic interactions between ZnO nanoparticles and the block copolymer template (Scheme 1). This mesostructured ZnO obtained after pyrolysis is compared to P25 in respect to the photodegradation efficiency of ciprofloxacin.

3. Materials and methods

3.1. Chemicals

If not mentioned otherwise, all chemicals were purchased from Sigma Aldrich, Germany and used as obtained.

3.2. Preparation of the block copolymer template

The polybutadiene-*block*-poly(2-vinylpyridine) (BV) diblock copolymer precursor used for the preparation of cylindrical polymer brushes (CPBs) was synthesized via living anionic polymerization in THF. Details on the diblock copolymer synthesis can be found in the Supplementary Information. To obtain the positive charged CPBs first 1 g of diblock copolymer was dissolved in 20 mL chloroform with 0.1 g of the photoinitiator Lucirin TPO (BASF). The solvent was allowed to evaporate slowly and resulted in hexagonally packed cylinders of polybutadiene (PB) segments in a poly(2-vinylpyridine) (P2VP) matrix. The PB core of the CPBs in the cast film was crosslinked using a UV-lamp (each side 2 h). The crosslinked polymer film (1 g) was dissolved in 200 mL chloroform and a tenfold excess of iodomethane solution (99 %, 3 mL) was dropwise added. After one day the precipitated product was washed and freeze dried.

3.3. Preparation of ZnO nanoparticles

ZnO nanoparticles were synthesized following a slightly modified published protocol [24]. Zinc acetate dihydrate (8.76 g, 0.04 mol) was dissolved in boiling ethanol (400 mL, 10 min). Lithium hydroxide monohydrate (2.348 g, 0.056 mol) was dissolved in ethanol (400 mL, 15 min) using ultrasonification. The lithium hydroxide solution was added to the zinc acetate solution at room temperature and directly cooled to 0 °C. The resulting ZnO nanoparticles were purified by precipitation in *n*-heptane (4 L) and subsequently redispersed in ethanol (500 mL).

3.4. Preparation of ZnO nanotubes

In a typical ZnO/BV hybridmaterial synthesis (1 g) with a weight ratio of 4:1, the ZnO nanoparticle dispersion (800 mg ZnO) was dropwise added to the BV solution (200 mg, 1 g L^{-1} in DMSO). After 2 h the hybridmaterial was diaylized against DMSO and washed with DMSO and water.

Template removal was done in a tube furnace with a heating and cooling rate of 180 °C h^{-1} and a maximum temperature of 490 °C which was hold for 5 min.

3.5. Photocatalytical degradation tests

For photocatalytical degradation of ciprofloxacin, 14 mg of the catalyst were added on a glass microfiber filter (Whatman, 37 mm diameter). The filter was adjusted in a self-constructed continuous flow reactor (Scheme S1). A ciprofloxacin solution (0.4 L, 2×10^{-5} mol L^{-1}) circulated through the reactor with an irradiated volume of 0.1 L and a flow rate of 12 L h^{-1}. The remaining volume is necessary to maintain a continuous circulation of the ciprofloxacin solution. After every 5–15 min of irradiation with solar spectrum from a 300 W Xenon lamp using an AM1.5 filter (1000 W m^{-2}), the ciprofloxacin concentration was determined photometrically by UV–vis.

3.6. Instruments and measurements

Powder X-ray diffraction (PXRD) measurements were performed applying a STOE Stadi P diffractometer with CuK_α radiation, equipped with a Mythen 1 K silicon strip-detector. Rietveld analysis was performed with TOPAS Academic applying a fundamental parameters approach for profile fitting. Implemented macros were used to obtain crystallite sizes. Assuming spherical particles resulted in a volume weighted average crystallite size

Dynamic light scattering (DLS) measurements were performed with a Malvern Zetasizer NS measuring three times 20 s at room temperature.

Transmission electron microscopy (TEM) images were taken on a Zeiss CEM 922 at accelerating voltages of 200 kV. All samples with the exception of the polymer film were prepared on a copper grid (200 mesh) with a carbon film by drop coating from ethanolic solution. The polymer film was cut ultrathin (30–80 nm) with a Reichert-Jung Ultracut E equipped with a diamond knife.

Scanning electron microscopy (SEM) micrographs were measured with a scanning electron microscope, LEO 1530 FESEM, equipped with a field emission cathode. All samples were drop-coated on a silicon wafer and sputtered with platinum. Energy dispersive X-ray scattering was performed with 20 kV.

Determination of surface area with N_2 was conducted at 77 K on a Quantachrome Autosorb 1 after degassing the sample at 363 K for 12 h.

Photocatalytic measurements were done in a continuous flow reactor with a flow rate of 10 L h^{-1}. Irradiation was done using a LOT Quantum Design 300 W Xe Arc Lamp (LSN254) with an AM1.5 filter.

UV–vis absorption spectra were measured by a Varian Cary 300 spectrometer using Hellma precisions cells made of Quartz SUPRASIL (type 100-QS, light path 10 mm).

PZC of ZnO nanotubes was determined using a ParticleMetrix Stabisizer PMX 200C. 50 mg ZnO nanotubes in 10 mL water with a pH of 10.5 (adjusted with 0.01 M NaOH) were titrated with 0.05 M HCl until the streaming potential was 0.

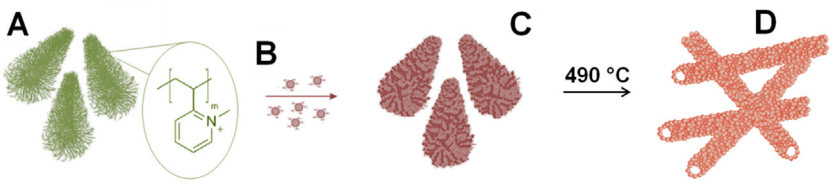

Scheme 1. (A) Methylated cationic cylindrical polymer brushes were loaded with (B) ZnO nanoparticles resulting in a (C) ZnO hybridmaterial that was (D) pyrolysed to mesostructured ZnO with a non-woven microstructure.

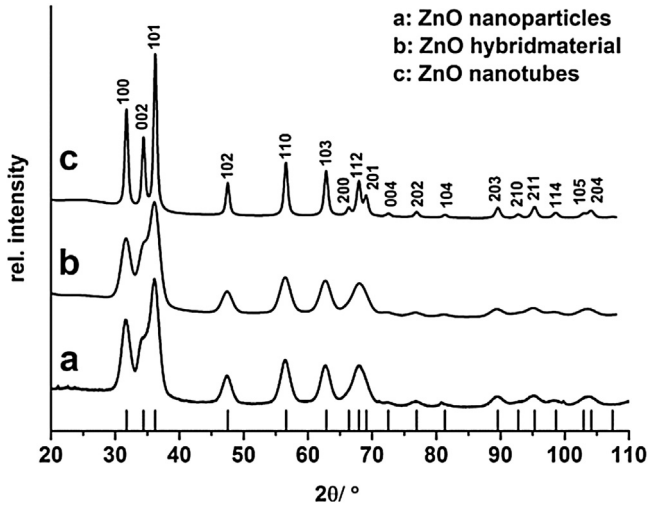

Fig. 1. PXRD pattern of (a) ZnO nanoparticles, (b) hybridmaterial and (c) after template removal with a reference of ZnO (vertical ticks PDF: 00-036-1451) and the Miller's indices.

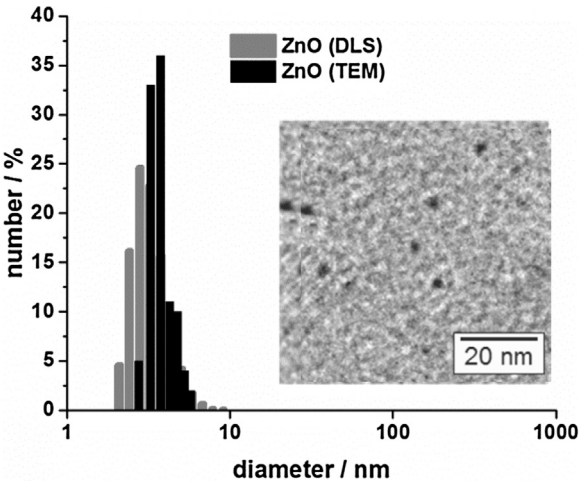

Fig. 2. Particle size distribution of ZnO nanoparticles determined by DLS measurements (dark grey) and TEM images (black). The inset shows a TEM image of ZnO nanoparticles.

4. Results and discussion

4.1. Characterization of the diblock copolymer template

The BV contained 19 wt% PB and had molar mass dispersity $\eth_M$ of 1.02 and molecular weight of 60,000 g mol^{-1} as determined by SEC (Fig. S1), MALDI-TOF and NMR (Fig. S2) experiments. This composition was chosen to obtain hexagonal PB cylinders in a P2VP matrix in the bulk state. A permanent positive charge of CPBs was obtained by redispersing the core-crossliked polymer film followed by methylation of the P2VP block. All steps were controlled by TEM micrographs (Fig. S3).

4.2. Characterization of ZnO nanoparticles

Phase purity of ZnO nanoparticles was confirmed by PXRD measurement (Fig. 1a). All peaks can be related to ZnO (marked by vertical ticks in Fig. 1; PDF: 00-036-1451) and the high full width at half maximum (FWHM) of the peaks indicates that nanoparticles were synthesized.

Particle size distributions of ZnO nanoparticles were determined independently by DLS (Fig. 2 dark grey) and TEM (Fig. 2 black). Average crystallite (coherently diffraction domain size) size was obtained by Rietveld analysis of PXRD measurement (Fig S4, Table S1) [25]. DLS gives a number weighted apparent hydrodynamic diameter of 3.2 nm. As expected, TEM (Fig 2 inset) and PXRD measurements give slightly different values. Examination of 100 nanoparticles using TEM micrographs yielded a median particle size of 2 nm. Rietveld analysis indicated coherent scattering domains of around 5 nm. TEM images and DLS measurements confirm that there was no aggregation or agglomeration of the nanoparticles.

4.3. Formation of ZnO nanotubes

ZnO nanoparticles are surface modified with acetate and therefore carry a negative charge that allows for a robust hybrid formation driven by electrostatic interactions with the positively charged CPBs [26]. As judged by the diffraction pattern, hybrid formation does not affect the crystallite size nor the phase purity (Fig. 1b). All peaks can be assigned to wurtzite. The CPBs are amorphous and contribute no peaks. Upon template removal by calcinations, the FWHM of the peaks decreases. As expected the nanocrystals grow during calcination but less than expected for a heat treatment at 490 °C. Rietveld refinements (Figs. S4–S6, Table S1–S3) yield in an average coherent scattering domain of 4.49(4)–5.05(4) nm for the nanoparticles, 4.21(5)–4.56(5) nm for the hybridmaterial and 12.0(1)–15.1(1) nm for calcinated material, respectively. Apparently the confinement to one dimension limits the crystallite growth.

The pristine unloaded CPBs have diameters of approximately 100 ± 11 nm and the PB core 30 ± 9 nm [27]. The diameter of the hybridmaterial is around 55 nm (Fig. 3). The contraction of the P2VP corona is in good agreement with similar work on TiO_2 hybrid formation [28]. The rods of hybridmaterial have high aspect ratio and the core shell structure was preserved (grey value analysis Fig. 3B inset). After drying of the hybridmaterial the wormlike character can still be observed and a non-woven microstructure is formed by self-assembly (Fig. 3A). The surface area of dried hybridmaterial determined by Brunauer–Emmett–Teller measurements with nitrogen physisorption was 44 m^2 g^{-1} (Fig. 4A).

Finally the loaded CPBs were calcinated in air at 490 °C. The polymer template was removed during temperature treatment. The nanorods are converted into nanotubes as evidenced by a grey scale analysis (Fig. 3C, D and inset). Elemental analysis proved that carbon was completely removed (less than 0.1%) during temperature

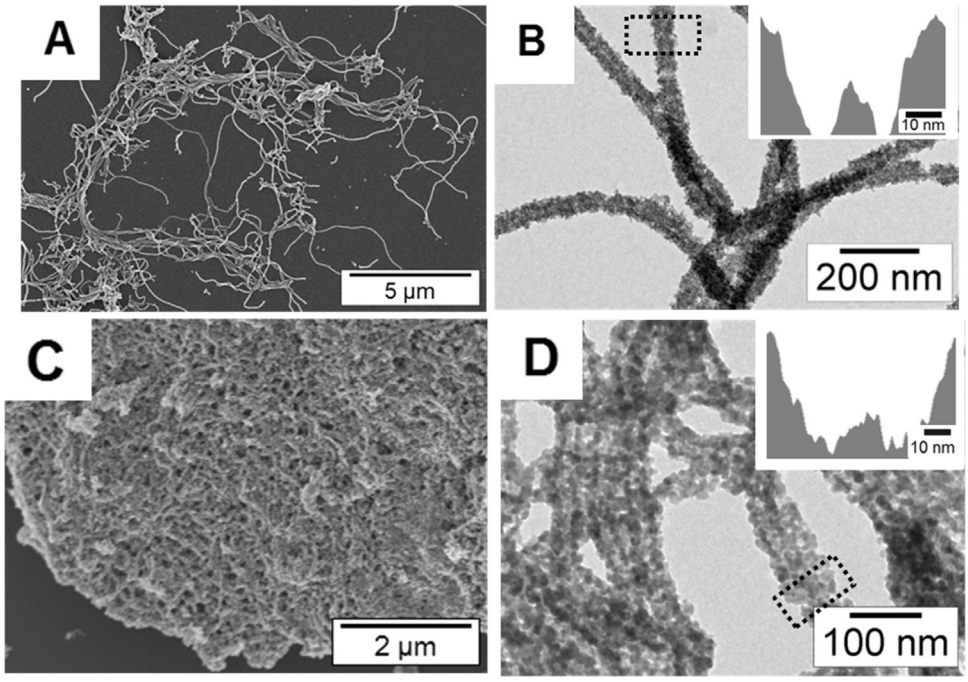

Fig. 3. (A) SEM and (B) TEM micrographs of the ZnO hybridmaterial; and (C) SEM and (D) TEM micrographs after template removal. Inset in B and D are grey value analyses performed with the package "image J".

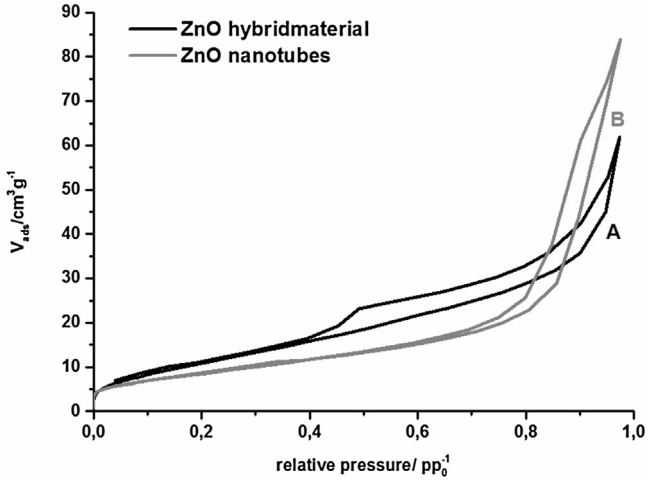

Fig. 4. N_2-sorption isotherm of (A) ZnO hybridmaterial (black) and (B) ZnO nanotubes (dark grey).

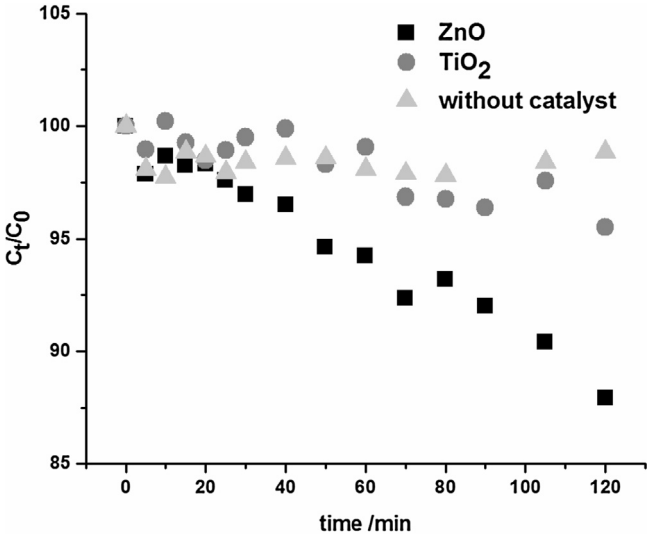

Fig. 5. Time dependent decrease of ciprofloxacin during irradiation with ZnO nanotubes (black squares), P25 (dark grey circles) and without catalyst (light grey triangles).

treatment. Due to the crystal growth, the surface area decreased from 44 m^2 g^{-1} to 31 m^2 g^{-1} (Fig. 4). The amount of ZnO was determined by EDX measurements to be 96 wt% for ZnO nanotubes (Fig. S8).

4.4. Photocatalytical degradation of ciprofloxacin

Preliminary test for photochemical wastewater treatment with the calcinated material demonstrated activity using a terrestrial solar spectrum. The bad gap of ZnO nanotubes was determined using UV–vis reflectance spectra of the powdered samples. The absorption data were calculated applying the Kubelka-Munk relation for diffuse reflectance data and yielded a band gap of 3.55 eV (Fig. S9) [29]. The PZC of 8.9 of synthesized ZnO nanotubes was determined by pH dependant streaming potential measurements and is in good agreement with the literature [21]. After an irradiation time of 120 min a comparative measurement without catalyst showed that ≈ 1% of ciprofloxacin was degraded (Fig. 5 light grey triangles). After an irradiation time of 120 min, ZnO nanotubes have degraded 12% of initial ciprofloxacin concentration (Fig. 5 black squares) while P25 degraded only 5% (Fig. 5 dark grey circles). In comparison with P25, the ZnO nanotube catalyst is significantly more efficient at pH 8. The higher efficiency is observed despite a lower surface area of mesostructured ZnO as compared to P25 (56 m^2 g^{-1}) [30].

The apparent rate constant k' can be calculated by the gradient of $\ln C_0/C_t = f(t)$ because the degradation follows a pseudo-first order kinetics. The k' value without catalyst equals 2.86×10^{-5} min^{-1}. ZnO nanotubes have a k' value of 9.61×10^{-4} min^{-1} as compared to P25 with k' = 3.36×10^{-4} min^{-1} (Fig. 6). Degradation with as little as 3.5 ppm of ZnO nanotubes is more than 33 times faster as with-

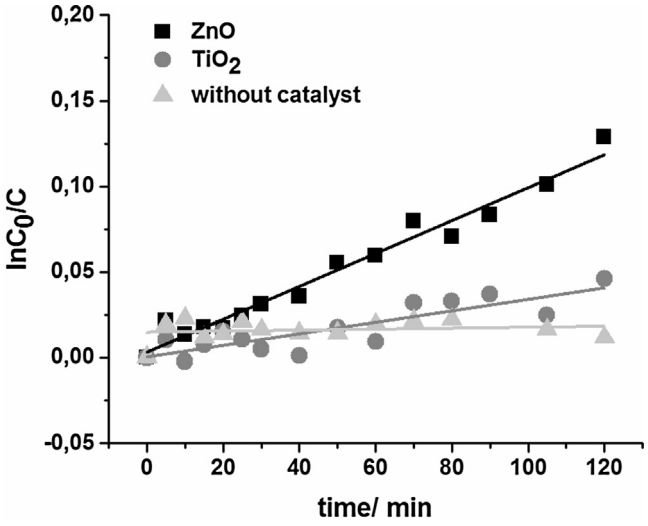

Fig. 6. First order kintics plots for ZnO nanotubes (black squares), P25 (dark grey circles) and without catalyst (light grey triangles).

out a catalyst. Compared to P25, ZnO nanotubes are 2.9 times more efficient. A possible explanation is the electrostatically favoured adsorption of ciprofloxacin on the positively charged ZnO surface as mentioned earlier. Obviously the photocatalytic degradation is also highly influenced by the separation of electron hole pairs [31]. Cavaleri et al. determined a decay time of 50 ps for ZnO nanocrystals of comparable size [32]. It has recently been shown for ZnO single crystals of varying habitus that the recombination probability is influenced by the aspect ratio and surface defects [33]. Mesostructuring of nanocrystalline ZnO into tubular structures as done here might influence both surface defects and aspect ratio and thus may have some influence on photocatalysis. This influence will be superimposed on the effect of surface charge discussed here to be advantageous for the degradation of ciprofloxacin by ZnO.

After the degradation tests, the filter with the ZnO nanotubes and the P25 catalyst was removed and dried. Both catalysts could be quantitatively recovered (14 mg and 13.6 mg of ZnO nanotubes and P25, respectively). No weight loss was observed in the technically benign continuous flow reactor. Contrary to ZnO nanoparticles the mesostructured ZnO nanotubes are big enough to remain completely on the glass microfiber filter. There is no need to use techniques like ultracentrifugation to separate and recycle the ZnO catalyst.

5. Conclusion

In conclusion, we were able to transfer our previous work on TiO_2 hybrid formation with negative charged CPBs on ZnO with positively charged CPBs [27,28,34–37]. At slightly basic pH, as typically found for hospital wastewater, basic ZnO was shown to be clearly superior to more acidic P25 in the photodegradation of ciprofloxacin, a model compound for wide-spread anionic pollutants due to its positive surface charge.

This colloidal route seems to be a general route for mesostructuring transition metal oxide nanoparticles. Even mixtures of different nanoparticles may be structured in the future. So this should allow for much better efficiency in the photocatalytical degradation by e.g. using ZnO and gold or silver nanoparticles.

The mesostructured ZnO with a non-woven microstructure was used in a continuous flow of wastewater applying a terrestrial solar spectrum. The mesostructured ZnO nanotubes showed good activity in degradation of ciprofloxacin and there was no loss of catalyst observed. Using P25 showed 2.9 times lower activity.

Acknowledgment

This work was funded by the Collaborative Research Center (SFB) 840.

Appendix A. Supplementary data

Supplementary data associated with this article can be found, in the online version, at http://dx.doi.org/10.1016/j.apcatb.2016.12.003.

References

[1] N.M. Vieno, H. Härkki, T. Tuhkanen, L. Kronberg, Environ. Sci. Technol. 41 (2007) 5077–5084.
[2] X. Van Doorslaer, K. Demeestere, P.M. Heynderickx, H. Van Langenhove, J. Dewulf, Appl. Catal. B: Environ. 101 (2011) 540–547.
[3] S. Gartiser, L. Brinker, T. Erbe, K. Kümmerer, R. Willmund, Acta Hydrochim. Hydrobiol. 24 (1996) 90–97.
[4] R. Lindberg, P.-Å. Jarnheimer, B. Olsen, M. Johansson, M. Tysklind, Chemosphere 57 (2004) 1479–1488.
[5] A. Cincinelli, T. Martellini, E. Coppini, D. Fibbi, A. Katsoyiannis, J. Nanosci. Nanotechnol. 15 (2015) 3333–3347.
[6] U.I. Gaya, A.H. Abdullah, J. Photochem. Photobiol. C: Photochem. Rev. 9 (2008) 1–12.
[7] N.S. Lewis, Science 315 (2007) 798–801.
[8] G. Rytwo, T. Klein, S. Margalit, O. Mor, A. Naftali, G. Daskal, Desalin. Water Treat. 57 (2016) 16424–16434.
[9] A. Kudo, Y. Miseki, Chem. Soc. Rev. 38 (2009) 253–278.
[10] K.M. Lee, C.W. Lai, K.S. Ngai, J.C. Juan, Water Res. 88 (2016) 428–448.
[11] I. Kazeminezhad, A. Sadollahkhani, Mater. Lett. 120 (2014) 267–270.
[12] Z.L. Wang, ACS Nano 2 (2008) 1987–1992.
[13] Ü Özgür, Y.I. Alivov, C. Liu, A. Teke, M.A. Reshchikov, S. Doğan, V. Avrutin, S.-J. Cho, H. Morkoc, J. Appl. Phys. 98 (2005) 41301–41404.
[14] A. Janotti, C.G. Van de Walle, Rep. Prog. Phys. 72 (2009) 126501–126531.
[15] A. Mclaren, T. Valdes-Solis, G. Li, S.C. Tsang, J. Am. Chem. Soc. 131 (2009) 12540–12541.
[16] M.A. Mohd Adnan, N.M. Julkapli, S.B. Abd Hamid, Rev. Inorg. Chem. 36 (2016) 77–104.
[17] J. Yu, X. Yu, Environ. Sci. Technol. 42 (2008) 4902–4907.
[18] L.J.M. Githinji, M.K. Musey, R.O. Ankumah, Water Air Soil Pollut. 219 (2011) 191–201.
[19] K. Torniainen, S. Tammilehto, V. Ulvi, Int. J. Pharm. 132 (1996) 53–61.
[20] C. Boillot, C. Bazin, F. Tissot-Guerraz, J. Droguet, M. Perraud, J.C. Cetre, D. Trepo, Y. Perrodin, Sci. Total Environ. 403 (2008) 113–129.
[21] M. Kosmulski, J. Colloid Interface Sci. 298 (2006) 730–741.
[22] M. Kosmulski, J. Colloid Interface Sci. 275 (2004) 214–224.
[23] N.T. Dung, N. Van Khoa, J.-M. Herrmann, Int. J. Photoenergy 7 (2005) 11–15.
[24] R. Marczak, F. Werner, J.-F. Gnichwitz, A. Hirsch, D.M. Guldi, W. Peukert, J. Phys. Chem. C 113 (2009) 4669–4678.
[25] G. Nabiyouni, M. Seraj, I. Kazeminezhad, B. Ghanbari, J. Mater. Sci. Mater. Electron. 26 (2015) 8047–8053.
[26] D. Yang, S. Tripathy, Y. Li, H.-J. Sue, Chem. Phys. Lett. 411 (2005) 150–154.
[27] M. Schieder, T. Lunkenbein, T. Martin, W. Milius, G. Auffermann, J. Breu, J. Mater. Chem. A 1 (2013) 381–387.
[28] M. Müllner, T. Lunkenbein, N. Miyajima, J. Breu, A.H.E. Müller, Small 8 (2012) 2636–2640.
[29] M.K. Debanath, S. Karmakar, Mater. Lett. 111 (2013) 116–119.
[30] K. Joseph, A. Raj, B. Viswanathan, Indian J. Chem. 48 (2009) 1378–1382.
[31] S. Ikeda, N. Sugiyama, B. Pal, G. Marcí, L. Palmisano, H. Noguchi, K. Uosaki, B. Ohtani, Phys. Chem. Chem. Phys. 3 (2001) 267–273.
[32] J.J. Cavaleri, D.E. Skinner, D.P. Colombo, R.M. Bowman, J. Chem. Phys. 103 (1995) 5378.
[33] X. Zhang, J. Qin, Y. Xue, P. Yu, B. Zhang, L. Wang, R. Liu, Sci. Rep. 4 (2014) 845–910.
[34] M. Müllner, T. Lunkenbein, M. Schieder, A.H. Gröschel, N. Miyajima, M. Förtsch, J. Breu, F. Caruso, A.H.E. Müller, Macromolecules 45 (2012) 6981–6988.
[35] M. Müllner, T. Lunkenbein, J. Breu, F. Caruso, A.H.E. Müller, Chem. Mater. 24 (2012) 1802–1810.
[36] M. Schieder, T. Lunkenbein, C. Bojer, M. Dulle, J. Vom Stein, G. Auffermann, T. Löbling, J. Schöbel, H. Schmalz, J. Breu, Z. Anorg. Allg. Chem. 641 (2015) 1829–1834.
[37] R.S. Yelamanchili, Y. Lu, T. Lunkenbein, N. Miyajima, L.T. Yan, M. Ballauff, J. Breu, Small 5 (2009) 1326–1333.